

# Quantum limit for two-dimensional resolution of two incoherent optical point sources

Shan Zheng Ang,<sup>1,\*</sup> Ranjith Nair,<sup>1</sup> and Mankei Tsang<sup>1,2,†</sup>

<sup>1</sup>*Department of Electrical and Computer Engineering,*

*National University of Singapore, 4 Engineering Drive 3, Singapore 117583*

<sup>2</sup>*Department of Physics, National University of Singapore, 2 Science Drive 3, Singapore 117551*

(Dated: May 12, 2022)

We obtain the multiple-parameter quantum Cramér-Rao bound for estimating the Cartesian components of the centroid and separation of two incoherent optical point sources using an imaging system with finite spatial bandwidth. Under quite general and realistic assumptions on the point-spread function of the imaging system, and for weak source strengths, we show that the Cramér-Rao bounds for the  $x$  and  $y$  components of the separation are independent of the values of those components, which may be well-below the conventional Rayleigh resolution limit. We also propose two linear optics-based measurement methods that approach the quantum bound for the estimation of the Cartesian components of the separation once the centroid has been located. One of the methods is an interferometric scheme that approaches the quantum bound for sub-Rayleigh separations. The other method uses fiber coupling to attain the bound regardless of the distance between the two sources.

## I. INTRODUCTION

Rayleigh's criterion for resolution of two incoherent point sources [1] has been the most accepted criterion for optical resolution since its formulation in 1879. In the past few decades, advances in far-field super-resolution techniques in microscopy [2–4] (see ref. [5] for a review) enable us to sidestep Rayleigh's limit. Still, as they require that nearby sources are not emitting at the same time, those technologies do not challenge Rayleigh's criterion fundamentally for independently emitting sources.

Being rooted in the optical measurement technology of its era, Rayleigh's criterion neglects the discrete and stochastic nature of the photodetection process. By adopting a stochastic framework, the studies [6–8] gave a modern formulation of the criterion for two sources radiating independently and incoherently. Using the Cramér-Rao (CR) bound of classical estimation theory [9], they showed that the localization accuracy of any unbiased estimator based on image-plane photon counting deteriorates rapidly on approaching sub-Rayleigh separations.

Very recently, the localization problem was reconsidered from the perspective of quantum estimation theory using the quantum Cramér-Rao (QCR) bound [10, 11]. Following a preliminary study of the fundamental localization limit in ref. [12], Tsang *et al.* [13] obtained the quantum limit on localizing two incoherent optical point sources in one-dimensional imaging. Their quantum bound is independent of separation and shows no deterioration when the two sources are closer than the conventional Rayleigh limit of the imaging system. Similar conclusions were reproduced using a semiclassical photodetection theory under a Poisson model [14]. In ref. [13], a linear optical measurement – SPADE (SPAtial-mode DEMultiplexing)—was also proposed and shown

to attain the QCR bound for any separation. Another measurement scheme proposed in ref. [15]—SLIVER (Super Localization by Image inVERsion interferometry)—approaches the QCR bound for sub-Rayleigh separations.

In this paper, motivated by the work in refs. [13, 15], we study the problem of two-dimensional localization of two incoherent optical point sources. We first obtain the full 4-parameter quantum Fisher information matrix characterizing the precision of estimating all four (transverse) Cartesian coordinates of the two sources. We then focus on estimating the separations in the  $x$  and  $y$  directions, which the QCR bounds are shown to be independent of. Recent theoretical studies in quantum parameter estimation proved the existence of a Positive-Operator Valued Measure (POVM) [10, 11] that achieves the QCR bound for estimation of a single parameter [16, 17], though the quantum bound may not be attainable for two or more parameters. Here we propose two measurement schemes which asymptotically attain the QCR bound for both components of the separation over many trials. The first is an extension of the SLIVER scheme for estimating both separation parameters and approaches the QCR bound for small values of source separation. The second is a two-dimensional version of the SPADE scheme that attains the bound regardless of the distance between the two sources.

This paper is organized as follows. In Sec. II, we define the source and system model used in this paper. In Sec. III, we review the multiparameter QCR bound and obtain from it the fundamental limit for the estimation of the Cartesian components of the centroid and separation of the sources. In Sections IV and V, the details of the above two proposed measurement schemes are discussed. In Sec. VI, we study the performance of the two schemes using Monte-Carlo simulations, and close with concluding remarks in Sec. VII.

\* eleasz@nus.edu.sg  
† mankei@nus.edu.sg

## II. SOURCE AND SYSTEM MODEL

We first lay out the source and imaging system model used in this paper, the former being identical to that in ref. [13]. We assume that two incoherent optical point sources with equal intensities are located on the object plane. Far-field radiation from these sources is collected at the entrance pupil of an optical imaging system such as a microscope or telescope. We assume that the paraxial approximation is valid for the field propagation from object plane to entrance pupil and consider a single polarization only. We further assume that the radiation from the sources is quasi-monochromatic and excites only a single temporal mode in order to focus on the spatial aspects of the resolution problem. We assume also that the imaging system is spatially-invariant [18], and that the image-plane coordinates  $(x, y)$  have been divided by the magnification factor and that  $\psi(x, y)$  is the two-dimensional point-spread function (PSF) of the system satisfying the normalization condition  $\int_{-\infty}^{\infty} dx \int_{-\infty}^{\infty} dy |\psi_s(x, y)|^2 = 1$  on the image plane.

We are given two incoherent optical point sources with equal intensities located at coordinates  $(X_1, Y_1)$  and  $(X_2, Y_2)$  on the object plane. We assume the two sources are weak enough so that the probability  $\epsilon$  of one or the other source (but not both) emitting one photon satisfies

$$\epsilon \ll 1. \quad (1)$$

We further assume that the probability of together emitting more than one photon is negligible. Under the above assumptions, the quantum density operator of the optical field on the image plane can be written as [13]

$$\rho = (1 - \epsilon)|\text{vac}\rangle\langle\text{vac}| + \frac{\epsilon}{2}(|\psi_1\rangle\langle\psi_1| + |\psi_2\rangle\langle\psi_2|), \quad (2)$$

where  $|\text{vac}\rangle$  denotes the vacuum state and states  $\{|\psi_s\rangle\}_{s=1}^2$  are given by

$$|\psi_s\rangle = \int_{-\infty}^{\infty} dx \int_{-\infty}^{\infty} dy \psi_s(x, y)|x, y\rangle, \quad s = 1, 2, \quad (3)$$

with the wavefunctions

$$\psi_s(x, y) = \psi(x - X_s, y - Y_s), \quad s = 1, 2, \quad (4)$$

and  $|x, y\rangle$  denotes the state with one photon in the mode corresponding to position  $(x, y)$  alone such that  $\langle x, y|x', y'\rangle = \delta(x - x')\delta(y - y')$ .

Eq. (2) means that a photon arrives with equal probability  $\epsilon/2$  from either of the two sources. If a photon arrives from the first source, it is in the state  $|\psi_1\rangle$  with wavefunction  $\psi_1(x, y)$ ; if it comes from the other source, it is in state  $|\psi_2\rangle$  with wavefunction  $\psi_2(x, y)$ . The two states are not orthogonal in general, with overlap

$$\delta \equiv \langle\psi_1|\psi_2\rangle = \int_{-\infty}^{\infty} dx \int_{-\infty}^{\infty} dy \psi_1^*(x, y)\psi_2(x, y) \neq 0. \quad (5)$$

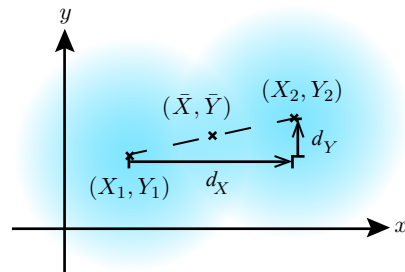


FIG. 1. An illustration of the focused image of two point sources centered at  $(X_1, Y_1)$  and  $(X_2, Y_2)$ . The shading indicates the approximate extent of the PSFs.

We also make a realistic simplifying assumption on the (possibly complex-valued) PSF  $\psi(x, y)$  of the imaging system, namely that it is symmetric about the origin (or inversion-symmetric), viz.,

$$\psi(x, y) = \psi(-x, -y). \quad (6)$$

This assumption is satisfied for most imaging systems of interest, including spatially-invariant systems whose entrance aperture is rectangular or (hard or apodized) circular in shape [18], and is more general than the assumption of a circularly-symmetric PSF used in ref. [15].

The parameters we are interested in estimating are the four components of the vector

$$\theta \equiv (\bar{X}, \bar{Y}, d_X, d_Y)^\top, \quad (7)$$

consisting of the centroid vector

$$(\bar{X}, \bar{Y}) = [(X_1, Y_1) + (X_2, Y_2)]/2, \quad (8)$$

and the separation vector

$$(d_X, d_Y) = (X_2, Y_2) - (X_1, Y_1), \quad (9)$$

as depicted in Fig. 1.

## III. THE QUANTUM LIMIT ON TWO-SOURCE LOCALIZATION

### A. Review of the multiparameter Quantum Cramér-Rao (QCR) bound

Let  $\rho_\theta$  be the density operator of a quantum system depending on an unknown vector parameter  $\theta$ . Consider the estimation of  $\theta$  from the quantum measurement outcome  $\mathcal{Y}$  on  $M$  copies of  $\rho_\theta$ . The probability distribution of  $\mathcal{Y}$  is given by

$$P(\mathcal{Y}) = \text{tr}[F(\mathcal{Y})\rho_\theta^{\otimes M}], \quad (10)$$

where  $F(\mathcal{Y})$  is the positive operator-valued measure (POVM) that characterizes the statistics of the quantum measurement [10, 19]. For any estimate  $\hat{\theta}(\mathcal{Y})$  of  $\theta$

from the measurement outcome, the estimation error covariance matrix has the matrix elements

$$\Sigma_{\mu\nu} \equiv \mathbb{E} \{ [\check{\theta}_\mu(\mathcal{Y}) - \theta_\mu] [\check{\theta}_\nu(\mathcal{Y}) - \theta_\nu] \}, \quad (11)$$

$$\mathbb{E}[z(\mathcal{Y})] \equiv \int d\mathcal{Y} P(\mathcal{Y}) z(\mathcal{Y}). \quad (12)$$

For any unbiased estimator, defined as one for which

$$\mathbb{E} [\check{\theta}(\mathcal{Y}) - \theta] = 0, \quad (13)$$

the error covariance matrix  $\Sigma$  is bounded by the classical and quantum Cramér-Rao bounds [9–11, 20],

$$\Sigma \geq j^{-1} \geq \mathcal{J}^{-1}. \quad (14)$$

Here, the inequalities mean that matrices  $\Sigma - j^{-1}$ ,  $\Sigma - \mathcal{J}^{-1}$  and  $j^{-1} - \mathcal{J}^{-1}$  are positive-semidefinite. Matrix  $j$  is the classical Fisher information matrix given by

$$j_{\mu\nu} = \mathbb{E} \left\{ \left[ \frac{\partial}{\partial \theta_\mu} \ln P(\mathcal{Y}) \right] \left[ \frac{\partial}{\partial \theta_\nu} \ln P(\mathcal{Y}) \right] \right\}, \quad (15)$$

and matrix  $\mathcal{J}$  is the quantum Fisher information (QFI) matrix which can be expressed in terms of the so-called symmetric logarithmic derivative (SLD) operators  $\{\mathcal{L}_\mu\}$  as

$$\mathcal{J}_{\mu\nu} = M \text{tr} \frac{\mathcal{L}_\mu \mathcal{L}_\nu + \mathcal{L}_\nu \mathcal{L}_\mu}{2} \rho_\theta. \quad (16)$$

If  $\rho_\theta$  is diagonalized in an orthogonal basis  $\{|e_n\rangle\}$ , viz.,  $\rho_\theta = \sum_n D_n |e_n\rangle\langle e_n|$ ,  $\mathcal{L}_\mu$  can be expressed as [20]

$$\mathcal{L}_\mu = \sum_{\substack{m,n \\ D_m + D_n \neq 0}} \frac{2}{D_m + D_n} \langle e_m | \frac{\partial \rho_\theta}{\partial \theta_\mu} | e_n \rangle |e_m\rangle\langle e_n|. \quad (17)$$

## B. Quantum Fisher Information (QFI) Matrix for two-source localization

We now consider the problem of estimation of the centroid and separation vectors for two incoherent point sources under the model of Section II. Assuming the quantum density operator of Eq. (2) and the inversion-symmetry of the PSF (Eq. (6)), Eqs. (16) and (17), the QFI matrix  $\mathcal{J}$  can be evaluated. Included in Appendix A are the salient details in the derivation of  $\mathcal{J}$ : the basis  $\{|e_n\rangle\}$  in which  $\rho$  is diagonal, its eigenvalues  $\{D_n\}$ , and the SLD operators. The quantum Fisher information in terms of  $\theta$  defined in Eq. (7) is found to be

$$\mathcal{J} = N \begin{pmatrix} 4(\Delta k_X^2 - \gamma_X^2) & 4(\alpha - \gamma_X \gamma_Y) & 0 & 0 \\ 4(\alpha - \gamma_X \gamma_Y) & 4(\Delta k_Y^2 - \gamma_Y^2) & 0 & 0 \\ 0 & 0 & \Delta k_X^2 & \alpha \\ 0 & 0 & \alpha & \Delta k_Y^2 \end{pmatrix}, \quad (18)$$

where  $N = M\epsilon$  is the average photon number collected over  $M$  trials, and

$$\begin{aligned} \Delta k_X^2 &\equiv \int_{-\infty}^{\infty} dx \int_{-\infty}^{\infty} dy \left| \frac{\partial \psi(x, y)}{\partial x} \right|^2, \\ \Delta k_Y^2 &\equiv \int_{-\infty}^{\infty} dx \int_{-\infty}^{\infty} dy \left| \frac{\partial \psi(x, y)}{\partial y} \right|^2, \\ \gamma_X &\equiv \int_{-\infty}^{\infty} dx \int_{-\infty}^{\infty} dy \psi^*(x - d_X, y - d_Y) \frac{\partial \psi(x, y)}{\partial x}, \\ \gamma_Y &\equiv \int_{-\infty}^{\infty} dx \int_{-\infty}^{\infty} dy \psi^*(x - d_X, y - d_Y) \frac{\partial \psi(x, y)}{\partial y}, \\ \alpha &= \text{Re} \left[ \int_{-\infty}^{\infty} dx \int_{-\infty}^{\infty} dy \frac{\partial \psi^*(x, y)}{\partial x} \frac{\partial \psi(x, y)}{\partial y} \right], \quad (19) \end{aligned}$$

for  $\text{Re}(z)$  denoting the real part of  $z$ . The terms  $\Delta k_X$  and  $\Delta k_Y$  are related to the spatial spectral width of the PSF in  $x$ - and  $y$ -direction, respectively and, along with  $\alpha$ , are independent of the source parameters  $\theta$ .  $\gamma_X$  and  $\gamma_Y$  depend on the separation coordinates  $(d_X, d_Y)$  but not on the centroid coordinates  $(\bar{X}, \bar{Y})$ . Thus,  $\mathcal{J}$  as a whole is independent of  $(\bar{X}, \bar{Y})$ , as may be expected from our assumption of a spatially-invariant imaging system. Note that  $\mathcal{J}$  has a block-diagonal form with respect to the centroid and separation coordinate pairs, and that the matrix elements related to the estimation errors of separations  $d_X$  and  $d_Y$ — $\mathcal{J}_{33}$  and  $\mathcal{J}_{44}$ —are independent of  $(d_X, d_Y)$  as well.

The QFI matrix can be simplified further for the case of a circularly-symmetric PSF  $\psi(x, y)$ , for which  $\alpha$  vanishes and

$$\Delta k_X = \Delta k_Y \equiv \Delta k, \quad (20)$$

so that  $\mathcal{J}$  becomes

$$\mathcal{J} = N \begin{pmatrix} 4(\Delta k^2 - \gamma_X^2) & -4\gamma_X \gamma_Y & 0 & 0 \\ -4\gamma_X \gamma_Y & 4(\Delta k^2 - \gamma_Y^2) & 0 & 0 \\ 0 & 0 & \Delta k^2 & 0 \\ 0 & 0 & 0 & \Delta k^2 \end{pmatrix}. \quad (21)$$

In Sections IV and V, we discuss concrete measurement schemes to simultaneously estimate the separation parameters  $\eta = (d_X, d_Y)^\top$ . For these schemes, we assume that the centroid  $(\bar{X}, \bar{Y})$  has already been located, and compare their performance to the quantum bound obtained here.

## IV. SUPER LOCALIZATION BY IMAGE INVERSION (SLIVER) INTERFEROMETRY

We now propose a two-stage interferometric scheme for estimation of  $d_X$  and  $d_Y$  adapting the SLIVER scheme of ref. [15]. The scheme is analyzed in the framework of quantum theory under weak-source condition; while the analysis in ref. [15] is of semiclassical photodetection theory [21, 22].

Assuming that the centroid of the sources is imaged at the origin of image-plane coordinates, the images of the sources are centered at  $\mp \frac{1}{2}(d_X, d_Y)$  in the image plane. The quantum density operator of Eq. (2) is thus

$$\rho = (1 - \epsilon_1 - \epsilon_2)|\text{vac}\rangle\langle\text{vac}| + \epsilon_1|\psi_1\rangle\langle\psi_1| + \epsilon_2|\psi_2\rangle\langle\psi_2|, \quad (22)$$

where  $\epsilon_1$  and  $\epsilon_2$  are the source intensities for source 1 and 2, respectively,  $|\text{vac}\rangle$  denotes the vacuum state and states  $\{|\psi_s\rangle\}_{s=1}^2$  are given by Eq. (3) with the wavefunctions

$$\psi_1(x, y) = \psi\left(x + \frac{d_X}{2}, y + \frac{d_Y}{2}\right), \quad (23)$$

$$\psi_2(x, y) = \psi\left(x - \frac{d_X}{2}, y - \frac{d_Y}{2}\right). \quad (24)$$

In this section, we relax the assumption of Sec. II that the two sources are of equal strength.

The scheme consists of two stages as illustrated in Fig. 2. The first stage involves the separation of the input field  $E(x, y)$  into antisymmetric ( $E_1$ ) and symmetric ( $E_S$ ) parts with respect to reflection about the  $y$ -axis. The symmetric and antisymmetric field components can be obtained by splitting the input field  $E(x, y)$  using a 50-50 beamsplitter, inverting the  $x$ -coordinates of the field (i.e., reflecting the field about the  $y$ -axis) from one output and recombining the two beams at a second 50-50 beamsplitter. The optics of the first stage thus consists of a balanced Mach-Zehnder interferometer with an extra reflection at an appropriately aligned plane mirror in one arm. Consider the quantum treatment of beamsplitter input-output relations, the output field operators are given by

$$E_1(x, y) = \frac{1}{2}\{[E(x, y) - E(-x, y)] + [V_1(x, y) + V_1(-x, y)]\}, \quad (25)$$

$$E_S(x, y) = \frac{1}{2}\{[E(x, y) + E(-x, y)] + [V_1(x, y) - V_1(-x, y)]\}, \quad (26)$$

where  $V_1(x, y)$  is the field operator at the open port of the first beamsplitter. At the antisymmetric output port with the field pattern of Eq. (25), an on-off non-spatially-resolving (bucket) detector is placed to distinguish between no photon and one photon. The measurement outcome  $g^{(1)}$  is binary – zero if the detector does not click and one if it does.

In the second stage, the output beam  $E_S(x, y)$  of the symmetric port is used as input to a second interferometer which similarly splits the field into antisymmetric ( $E_2$ ) and symmetric ( $E_3$ ) components with respect to reflection about the  $x$ -axis. The output field operators are

given by

$$E_2(x, y) = \frac{1}{2}[E_S(x, y) - E_S(x, -y)] + [V_2(x, y) + V_2(x, -y)], \quad (27)$$

$$E_3(x, y) = \frac{1}{2}\{[E_S(x, y) + E_S(x, -y)] + [V_2(x, y) - V_2(x, -y)]\}, \quad (28)$$

where  $V_2(x, y)$  is the field operator at the open port of the first beamsplitter in this stage. The output fields  $E_2$  and  $E_3$  of this stage impinge upon two individual on-off bucket detectors to give measurement outcomes  $g^{(2)}$  and  $g^{(3)}$ , respectively. As in the previous stage, binary outcomes  $g^{(2)}$  and  $g^{(3)} - 0$  if the corresponding detector does not click and 1 if it does – are recorded.

The expected photon number at the  $r$ th detector is  $\text{tr}(\rho N_r)$  where the total-photon-number operator

$$N_r = \int_{-\infty}^{\infty} dx \int_{-\infty}^{\infty} dy E_r^\dagger(x, y) E_r(x, y), \quad r = 1, 2, 3. \quad (29)$$

Our assumption of negligible probability for multiple photon emission event ensures that at most one photon will impinge upon any of the three photodetectors. There are no valid cases of having more than one detector clicks; in the event of a detector click, only one photon impinge upon it. Therefore, there are only four mutually exclusive measurement outcomes. Probability  $P(0)$  corresponds to the case where no photon detected in any of the three detectors and probability  $P(r)$  corresponds to the case where only the  $r$ th detector clicks, i.e.,

$$\begin{aligned} P(0) &= \Pr[g^{(1)} = 0, g^{(2)} = 0, g^{(3)} = 0], \\ P(1) &= \Pr[g^{(1)} = 1, g^{(2)} = 0, g^{(3)} = 0], \\ P(2) &= \Pr[g^{(1)} = 0, g^{(2)} = 1, g^{(3)} = 0], \\ P(3) &= \Pr[g^{(1)} = 0, g^{(2)} = 0, g^{(3)} = 1]. \end{aligned} \quad (30)$$

Since either zero or one photon arrives at each detector, the probability of only the  $r$ th detector clicks is equal to the expected photon number at the  $r$ th detector, i.e.,

$$P(r) = \text{tr}(\rho N_r). \quad (31)$$

Included in Appendix B is the detail evaluation of this trace operation, and the results are

$$\begin{aligned} P(1) &= \frac{\epsilon}{2}(1 - \delta_x), \\ P(2) &= \frac{\epsilon}{4}(1 + \delta_x - \delta_y - \delta), \\ P(3) &= \frac{\epsilon}{4}(1 + \delta_x + \delta_y + \delta), \end{aligned} \quad (32)$$

and no-click probability  $P(0) = 1 - \epsilon$ . Here,  $\epsilon = \epsilon_1 + \epsilon_2$  is the total source intensity,

$$\delta_x = \int_{-\infty}^{\infty} dx \int_{-\infty}^{\infty} dy \psi^*(x, y) \psi(x - d_X, y), \quad (33)$$

$$\delta_y = \int_{-\infty}^{\infty} dx \int_{-\infty}^{\infty} dy \psi^*(x, y) \psi(x, y - d_Y), \quad (34)$$

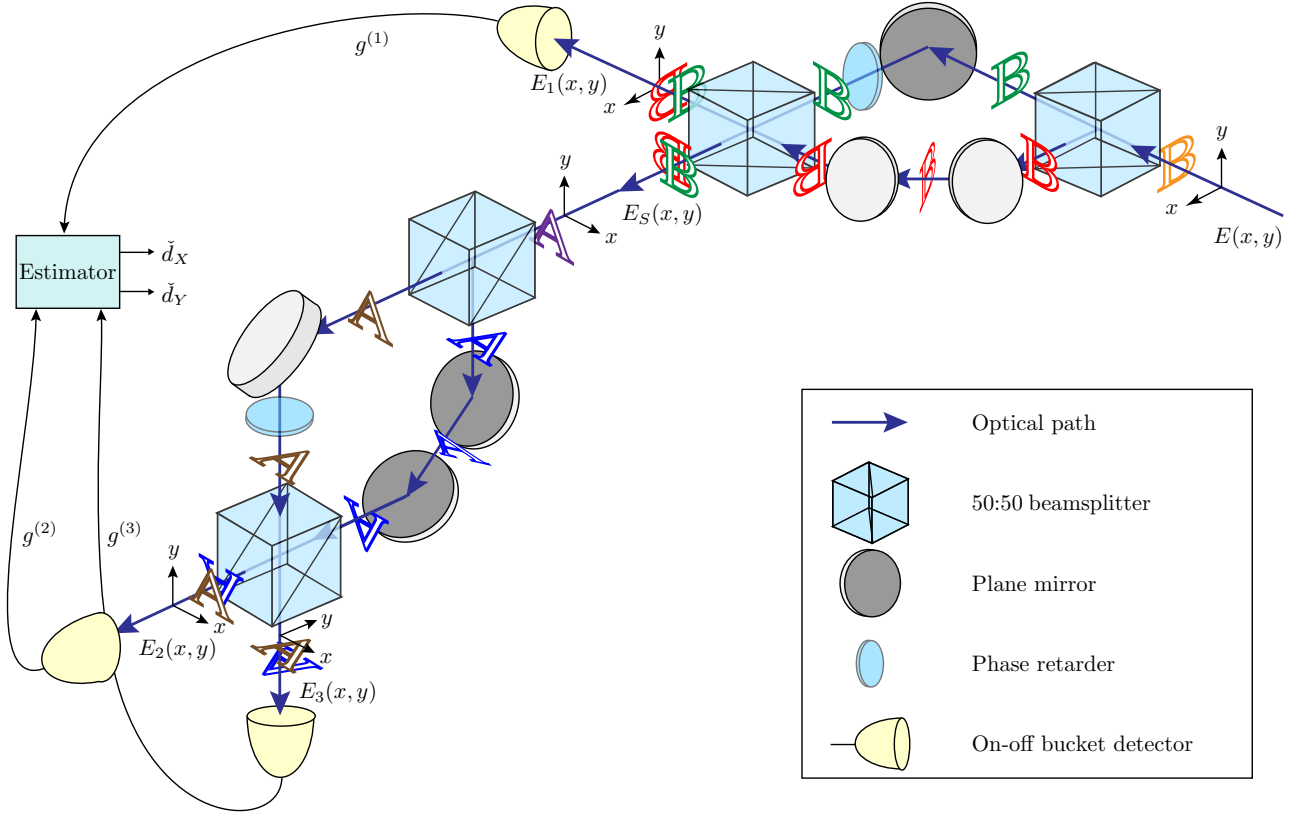


FIG. 2. A schematic of 2-stage SLIVER – The input field  $E(x, y)$  is separated into symmetric ( $E_S$ ) and antisymmetric ( $E_X$ ) components with respect to reflection about the  $y$ -axis. The  $E_X$  component impinges upon a bucket photodetector. The  $E_S$  component is separated again into symmetric and antisymmetric ( $E_Y$ ) components with respect to reflection about the  $x$ -axis, and the  $E_Y$  component impinges upon a second bucket detector. These field transformations are realized by the extra reflection at an appropriately aligned plane mirror in one arm of the balanced Mach-Zehnder interferometers. The set of binary outcomes,  $g_X$  and  $g_Y$ , observed in the detectors over a series of  $M$  measurements is processed to give estimates  $\hat{d}_X$  and  $\hat{d}_Y$  of the components of the separation. The letters  $\mathbb{A}$  and  $\mathbb{B}$  illustrate the reflection of the field.

and  $\delta$  is given by Eq. (5).

The Fisher information matrix  $j^{(\text{SLI})}$  for the separation vector  $\eta = (d_X, d_Y)^\top$  using SLIVER is given by

$$j_{\mu\nu}^{(\text{SLI})} = \sum_{r=1}^3 P(r) \frac{\partial P(r)}{\partial \eta_\mu} \frac{\partial P(r)}{\partial \eta_\nu}, \quad \mu, \nu = 1, 2. \quad (35)$$

Using Eqs. (35) and (32), we evaluate the Fisher information matrix and it has elements

$$\begin{aligned} j_{11}^{(\text{SLI})} &= \frac{\epsilon}{2} \left[ \frac{1}{1 - \delta_x} \left( \frac{\partial \delta_x}{\partial d_X} \right)^2 + \frac{1}{2(1 + \delta_x - \delta_y - \delta)} \left( \frac{\partial \delta_x}{\partial d_X} - \frac{\partial \delta}{\partial d_X} \right)^2 + \frac{1}{2(1 + \delta_x + \delta_y + \delta)} \left( \frac{\partial \delta_x}{\partial d_X} + \frac{\partial \delta}{\partial d_X} \right)^2 \right], \\ j_{22}^{(\text{SLI})} &= \frac{\epsilon}{4} \left[ \frac{1}{1 + \delta_x - \delta_y - \delta} \left( \frac{\partial \delta_y}{\partial d_Y} + \frac{\partial \delta}{\partial d_Y} \right)^2 + \frac{1}{1 + \delta_x + \delta_y + \delta} \left( \frac{\partial \delta_y}{\partial d_Y} - \frac{\partial \delta}{\partial d_Y} \right)^2 \right], \\ j_{12}^{(\text{SLI})} &= \frac{\epsilon}{4} \left[ \frac{1}{1 + \delta_x + \delta_y + \delta} \left( \frac{\partial \delta_x}{\partial d_X} + \frac{\partial \delta}{\partial d_X} \right) \left( \frac{\partial \delta_y}{\partial d_Y} + \frac{\partial \delta}{\partial d_Y} \right) - \frac{1}{1 + \delta_x - \delta_y - \delta} \left( \frac{\partial \delta_x}{\partial d_X} - \frac{\partial \delta}{\partial d_X} \right) \left( \frac{\partial \delta_y}{\partial d_Y} + \frac{\partial \delta}{\partial d_Y} \right) \right] \\ &= j_{21}^{(\text{SLI})}. \end{aligned} \quad (36)$$

We illustrate the above results for a circular Gaussian PSF

$$\psi(x, y) = \left( \frac{1}{2\pi\sigma^2} \right)^{1/2} \exp \left( -\frac{x^2 + y^2}{4\sigma^2} \right). \quad (37)$$

The PSF-dependent quantities appearing in the Fisher information are

$$\begin{aligned} \delta &= \delta_x \delta_y, \\ \delta_x &= \exp\left(-\frac{d_X^2}{8\sigma^2}\right), \quad \delta_y = \exp\left(-\frac{d_Y^2}{8\sigma^2}\right), \\ \frac{\partial \delta_x}{\partial d_X} &= -\frac{d_X}{4\sigma^2} \exp\left(-\frac{d_X^2}{8\sigma^2}\right), \\ \frac{\partial \delta_y}{\partial d_Y} &= -\frac{d_Y}{4\sigma^2} \exp\left(-\frac{d_Y^2}{8\sigma^2}\right), \\ \frac{\partial \delta}{\partial d_X} &= \delta_y \frac{\partial \delta_x}{\partial d_X}, \quad \frac{\partial \delta}{\partial d_Y} = \delta_x \frac{\partial \delta_y}{\partial d_Y}. \end{aligned} \quad (38)$$

In this example, the Fisher information matrix  $j^{(\text{SLI})}$  has elements

$$\begin{aligned} j_{11}^{(\text{SLI})} &= \frac{\epsilon}{1 - \delta_x^2} \left( \frac{\partial \delta_x}{\partial d_X} \right)^2, \\ j_{22}^{(\text{SLI})} &= \frac{\epsilon}{1 - \delta_y^2} \frac{1 + \delta_x}{2} \left( \frac{\partial \delta_y}{\partial d_Y} \right)^2, \\ j_{12}^{(\text{SLI})} &= j_{21}^{(\text{SLI})} = 0. \end{aligned} \quad (39)$$

As  $d_X, d_Y \rightarrow 0$ , matrix elements approach

$$\begin{aligned} j_{11}^{(\text{SLI})} &\rightarrow \epsilon \Delta k^2 = \mathcal{J}_{33}, \\ j_{22}^{(\text{SLI})} &\rightarrow \epsilon \Delta k^2 = \mathcal{J}_{44}, \end{aligned} \quad (40)$$

where  $\Delta k^2 = (4\sigma^2)^{-1}$ . The Fisher information elements  $j_{11}^{(\text{SLI})}$  and  $j_{22}^{(\text{SLI})}$  of Eq. (39) are plotted as a function of separation parameters  $d_X$  and  $d_Y$  in Fig. 3. The total source strength  $\epsilon = 2 \times 10^{-3}$  photons. The plots are normalized to  $\epsilon \Delta k^2$ , the values of  $\mathcal{J}_{33}$  and  $\mathcal{J}_{44}$ . We see that the maximum values of  $j_{11}^{(\text{SLI})}$  and  $j_{22}^{(\text{SLI})}$ , attained at  $d_X = d_Y = 0$ , are equal to the value of QCR bound as shown in Eq. (40). Fig. 3(a) suggests that the Fisher information on  $d_X - j_{11}^{(\text{SLI})}$  – remains unchanged despite variation in  $d_Y$ , while the Fisher information on  $d_Y - j_{22}^{(\text{SLI})}$  – depends on values of both  $d_X$  and  $d_Y$  as depicted in Fig. 3(b). This asymmetry is a consequence of our estimating  $d_X$  in the first stage of the scheme and  $d_Y$  in the second.

A simpler non-cascaded version of the scheme may be envisaged in which the input field  $E(x, y)$  is split using a 50:50 beamsplitter, and the two outputs are used to separately estimate  $d_X$  and  $d_Y$ . Though it treats the separation components symmetrically, such a setup can only approach half of the QCR bound for each component due to the energy splitting. On the other hand, in the cascaded scheme given here, if  $d_X \approx 0$ ,  $E_X(x, y) \approx 0$ , and  $E_S(x, y) \approx E(x, y)$ , so that the first stage taps only a small fraction of the available energy (the energy loss is zero if  $d_X = 0$ ). This enables  $d_Y$  to be estimated in the second stage with little loss of energy to the first stage, and allows approaching the QCR bound for sub-Rayleigh separations.

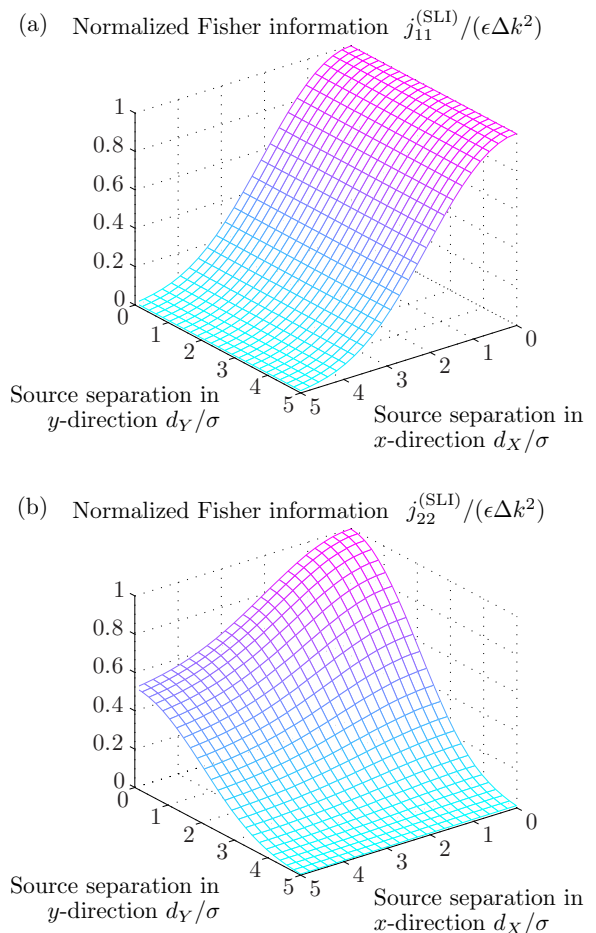


FIG. 3. The (classical) Fisher information matrix  $j^{\text{SLI}}$  for the SLIVER scheme as a function of the source separation  $(d_X, d_Y)$ . (a) Fisher information for  $x$ -separation  $j_{11}^{(\text{SLI})}$ . (b) Fisher information for  $y$ -separation  $j_{22}^{(\text{SLI})}$ . The plots are normalized with respect to the value  $\epsilon \Delta k^2$  of  $\mathcal{J}_{33}$  and  $\mathcal{J}_{44}$ . The quantum bound is attained at  $d_X = d_Y = 0$  as illustrated in (a) and (b). The circular Gaussian PSF of Eq. (37) is assumed, with the total source strength  $\epsilon = 2 \times 10^{-3}$  photons.

## V. SPATIAL-MODE DEMULTIPLEXING (SPADE)

We now generalize the SPADE scheme of ref. [13] to the estimation of the vector separation. In the derivation of the QFI matrix  $\mathcal{J}$  in Sec. III, we worked in the orthonormal basis given by Eq. (A4). Now consider the discrete Hermite-Gaussian (HG) basis  $\{|\phi_{qr}\rangle; q, r = 0, 1, \dots\}$  for the one-photon subspace, where

$$|\phi_{qr}\rangle = \int_{-\infty}^{\infty} dx \int_{-\infty}^{\infty} dy \phi_{qr}(x, y) |x, y\rangle, \quad (41)$$

$$\begin{aligned} \phi_{qr}(x, y) &= \left( \frac{1}{2\pi\sigma_X\sigma_Y} \right)^{1/2} \frac{1}{\sqrt{2^{q+r}q!r!}} H_q \left( \frac{x}{\sqrt{2}\sigma_X} \right) \\ &\quad \times H_r \left( \frac{y}{\sqrt{2}\sigma_Y} \right) \exp \left( -\frac{x^2}{4\sigma_X^2} - \frac{y^2}{4\sigma_Y^2} \right), \end{aligned} \quad (42)$$

$H_q$  and  $H_r$  are the Hermite polynomials [23], and  $q, r = 0, 1, \dots$ . Consider the POVM consisting of the projections

$$W_0 = |\text{vac}\rangle\langle\text{vac}|, \quad (43)$$

$$W_1(q, r) = |\phi_{qr}\rangle\langle\phi_{qr}|, \quad q, r = 0, 1, \dots \quad (44)$$

We further assume that the PSF is circular Gaussian as in Eq. (37). The image-plane field in Eq. (2) is scaled in one direction with a series of mirrors such that the PSF is now of the elliptical Gaussian form

$$\psi'(x, y) = \left(\frac{1}{2\pi\sigma_X\sigma_Y}\right)^{1/2} \exp\left(-\frac{x^2}{4\sigma_X^2} - \frac{y^2}{4\sigma_Y^2}\right) \quad (45)$$

$$= \phi_{00}(x, y), \quad (46)$$

where  $\sigma_X = \sigma$  and  $\sigma_Y = s\sigma$ . The above POVM, if performed on the resulting density operator  $\rho'$ , has the outcome probabilities

$$P_0 \equiv \text{tr}(W_0\rho') = 1 - \epsilon, \quad (47)$$

$$P_1(q, r) \equiv \text{tr}[W_1(q, r)\rho'] \quad (48)$$

$$= \frac{\epsilon}{2} (|\langle\phi_{qr}|\psi'_1\rangle|^2 + |\langle\phi_{qr}|\psi'_2\rangle|^2). \quad (49)$$

If  $(\bar{X}, \bar{Y}) = (0, 0)$ , the wavefunctions become

$$\psi'_1(x, y) = \psi' \left( x + \frac{d_X}{2}, y + \frac{sd_Y}{2} \right), \quad (50)$$

$$\psi'_2(x, y) = \psi' \left( x - \frac{d_X}{2}, y - \frac{sd_Y}{2} \right), \quad (51)$$

and the overlaps in Eq. (49) are

$$|\langle\phi_{qr}|\psi'_1\rangle|^2 = \left| \int_{-\infty}^{\infty} dx \int_{-\infty}^{\infty} dy \phi_{qr}^*(x, y) \times \phi_{00} \left( x + \frac{d_X}{2}, y + \frac{sd_Y}{2} \right) \right|^2, \quad (52)$$

$$|\langle\phi_{qr}|\psi'_2\rangle|^2 = \left| \int_{-\infty}^{\infty} dx \int_{-\infty}^{\infty} dy \phi_{qr}^*(x, y) \times \phi_{00} \left( x - \frac{d_X}{2}, y - \frac{sd_Y}{2} \right) \right|^2. \quad (53)$$

Evaluate the integrals using properties of Hermite polynomials, we have

$$|\langle\phi_{qr}|\psi'_1\rangle|^2 = |\langle\phi_{qr}|\psi'_2\rangle|^2 = \exp(-Q - R) \frac{Q^q R^r}{q!r!}, \quad (54)$$

where

$$Q = \frac{d_X^2}{16\sigma^2}, \quad R = \frac{d_Y^2}{16\sigma^2}. \quad (55)$$

As the two integrals are equal, the probability

$$P_1(q, r) = \epsilon \exp(-Q - R) \frac{Q^q R^r}{q!r!} \quad (56)$$

is valid even if the two sources have unequal intensities. The Fisher information matrix for the HG-basis measurement on  $\eta = (d_X, d_Y)^\top$  can be found using Eq. (15), with elements

$$j_{11}^{(\text{HG})} = \sum_{q,r=0}^{\infty} P_1(q, r) \left[ \frac{\partial}{\partial d_X} \ln P_1(q, r) \right]^2 \quad (57)$$

$$= \frac{\epsilon}{Q} \left( \frac{\partial Q}{\partial d_X} \right)^2 = \frac{\epsilon}{4\sigma^2} = \mathcal{J}_{33}, \quad (58)$$

$$j_{22}^{(\text{HG})} = \sum_{q,r=0}^{\infty} P_1(q, r) \left[ \frac{\partial}{\partial d_Y} \ln P_1(q, r) \right]^2 \quad (59)$$

$$= \frac{\epsilon}{R} \left( \frac{\partial R}{\partial d_Y} \right)^2 = \frac{\epsilon}{4\sigma^2} = \mathcal{J}_{44}, \quad (60)$$

$$j_{12}^{(\text{HG})} = j_{21}^{(\text{HG})} = 0, \quad (61)$$

which equals the QFI matrix given by Eq. (21). This proves that the above measurement scheme using the HG basis is optimal for a Gaussian PSF.

A quadratic-index fiber can support the Hermite-Gaussian mode profiles [24]. To measure in the HG basis, the optical field is coupled into an elliptical multi-mode fiber supporting the modes in Eq. (42). Choosing the scaling factor  $s$  carefully (for example, an irrational number), each mode will have a distinct propagation constant  $\beta_{qr}$  along propagation direction  $z$ . On the other hand, a cylindrical fiber will result in degenerate propagation constant for modes of same order  $(q + r)$ . Each mode in the elliptic fiber is then coupled to different single-mode waveguides of specific propagation constant via evanescent coupling as illustrated in Fig. 4. The phase matching condition ensures that only one mode from the elliptic fiber is coupled to each waveguide, which are then detected using individual photon counter in the far-field.

## VI. MONTE-CARLO ANALYSIS OF SLIVER AND SPADE

To demonstrate that the two schemes can perform as predicted by their Cramér-Rao bounds, we study Monte-Carlo simulations of the mean-square error (MSE) for SLIVER and SPADE. The circular Gaussian PSF of Eq. (37) is assumed. Each MSE is computed by averaging over  $10^5$  Monte-Carlo runs.

### A. Monte-Carlo analysis of SLIVER

In  $M$  trials, consider direct detection of  $E_1(x, y)$ ,  $E_2(x, y)$  and  $E_3(x, y)$  using three on-off bucket detectors as in Fig. 2. The measurement record consists of the bitstrings  $(g_1^{(1)}, g_2^{(1)}, \dots, g_M^{(1)})$ ,  $(g_1^{(2)}, g_2^{(2)}, \dots, g_M^{(2)})$  and  $(g_1^{(3)}, g_2^{(3)}, \dots, g_M^{(3)})$ , where  $g_m^{(1)}$ ,  $g_m^{(2)}$  and  $g_m^{(3)}$  are zero (one) if the corresponding detector did not click (clicked) in the  $m$ -th trial.

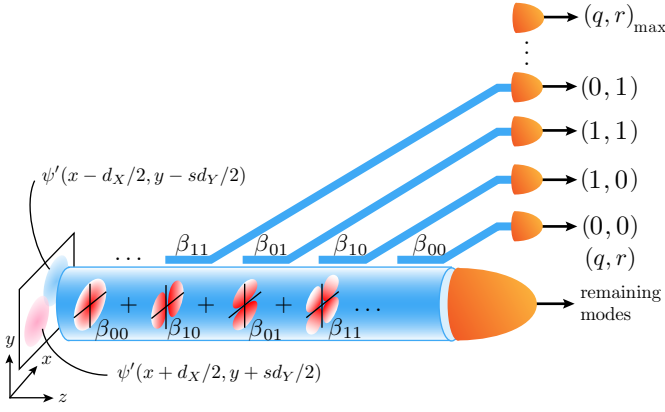


FIG. 4. A schematic of a multimode-fiber SPADE. The scaled field of Eq. (45) is coupled into an elliptical multimode fiber. With evanescent coupling, each mode is coupled to a single-mode waveguide of specific propagation constant and led to a photon counter. The photon counter at the end of the multimode fiber captures any remaining photon in the higher-order or leaky modes.

The total numbers of clicks observed in the three detectors over  $M$  measurements are, respectively,

$$G^{(1)} = \sum_{m=1}^M g_m^{(1)}, \quad G^{(2)} = \sum_{m=1}^M g_m^{(2)}, \quad G^{(3)} = \sum_{m=1}^M g_m^{(3)}, \quad (62)$$

and the total number of detected photons  $L = G^{(1)} + G^{(2)} + G^{(3)}$ . For estimation error analysis we can condition on  $L$ , which is obtained after an experiment, instead of the average photon number  $N$ ; the QCR bounds for estimation of  $d_X$  and  $d_Y$  become  $4\sigma^2/L$ . The maximum likelihood estimators for  $d_X$  and  $d_Y$  can be shown to be

$$\check{d}_X^{(\text{SLI})} = \begin{cases} 2\sigma \sqrt{-2 \ln \left(1 - \frac{2G^{(1)}}{L}\right)} & \text{if } \frac{2G^{(1)}}{L} < 1, \\ 2\sigma & \text{otherwise,} \end{cases}$$

$$\check{d}_Y^{(\text{SLI})} = \begin{cases} 2\sigma \sqrt{-2 \ln \left(1 - \frac{2G^{(2)}}{L-G^{(1)}}\right)} & \text{if } \frac{2G^{(2)}}{L-G^{(1)}} < 1, \\ 2\sigma & \text{otherwise.} \end{cases} \quad (63)$$

The second case for both  $\check{d}_X^{(\text{SLI})}$  and  $\check{d}_Y^{(\text{SLI})}$  is necessary because the logarithm function  $\ln(z)$  in the equations for the estimators is undefined for  $z \leq 0$ . The estimators are set to an arbitrary value if the argument of the logarithm goes negative, which happens with a probability tending to zero as  $L$  increases.

Figures 5 and 6 show the simulated MSEs of the ML estimators in Eq. (63) for  $\epsilon = 2 \times 10^{-3}$  photons. The simulated MSEs are plotted relative to the minimum value of the Cramér-Rao bound for that  $L$  at  $d_X = d_Y = 0$ . Fig. 5 plots the MSE of estimator  $\check{d}_X^{(\text{SLI})}$  as a function of  $x$ -separation for  $d_Y = 0$ , the ML estimator beats the

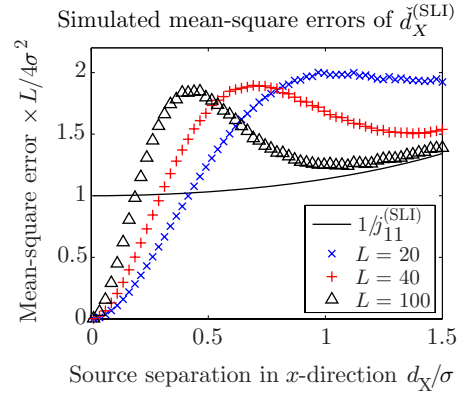


FIG. 5. Simulated mean-square errors of SLIVER with maximum likelihood estimator of Eq. (63). MSE of estimator  $\check{d}_X^{(\text{SLI})}$  as a function of the separation in  $x$ -direction for  $L = 20, 40, 100$  measurements and  $d_Y = 0$ .

Cramér-Rao bound for  $d_X/\sigma < 0.1$  due to the biasedness of the estimator. The MSE of estimator  $\check{d}_Y^{(\text{SLI})}$  as a function of  $y$ -separation for  $d_X = 0$  is virtually identical to that of Fig. 5 and is not shown. This behavior is expected as  $E_S(x, y) = E(x, y)$  if  $d_X = 0$ .

Figure 6 explores the dependence of the MSE of the ML estimators on the separations  $d_X$  – the number of measurements  $L = 100$  and the corresponding Cramér-Rao bounds for the relevant separations are shown. Fig. 6(a) shows the simulated MSE of estimator  $\check{d}_X^{(\text{SLI})}$  as a function of  $d_X$ , for  $d_Y = 0, 0.74\sigma$ , and  $1.5\sigma$ . We see that both the estimator and the Cramér-Rao bound show little dependence on the separation  $d_Y$ . Fig. 6(b) plots the simulated MSE of estimator  $\check{d}_Y^{(\text{SLI})}$  against  $d_Y$  for the case of  $d_X = 0, 0.74\sigma$ , and  $1.5\sigma$ . As  $d_X$  increases, the Cramér-Rao bound increases along with the MSE of the estimator.

## B. Monte-Carlo analysis of SPADE with maximum-likelihood estimation

After  $M$  trials of the SPADE measurement of Sec. V, the total number  $L$  of detected photons is known, and for estimation error analysis we can condition on  $L$  instead of the average photon number  $N$ . Then the QCR bounds for estimation of  $d_X$  and  $d_Y$  become  $4\sigma^2/L$ .

Each photon collected by the imaging system triggers precisely one photon detector indexed by the HG mode index  $(q, r)$ . Let the mode excited by the  $l$ -th photon be denoted  $(q_l, r_l)$ , for  $1 \leq l \leq L$ . The maximum likelihood estimators for  $d_X$  and  $d_Y$  can be shown to be

$$\check{d}_X^{(\text{SPA})} = 4\sigma \sqrt{\frac{H_X}{L}}, \quad \check{d}_Y^{(\text{SPA})} = 4\sigma \sqrt{\frac{H_Y}{L}}. \quad (64)$$

where  $H_X = \sum_{l=0}^L q_l$  and  $H_Y = \sum_{l=0}^L r_l$ . Fig. 7(a) and (b) show the results for the MSE of the ML estimators

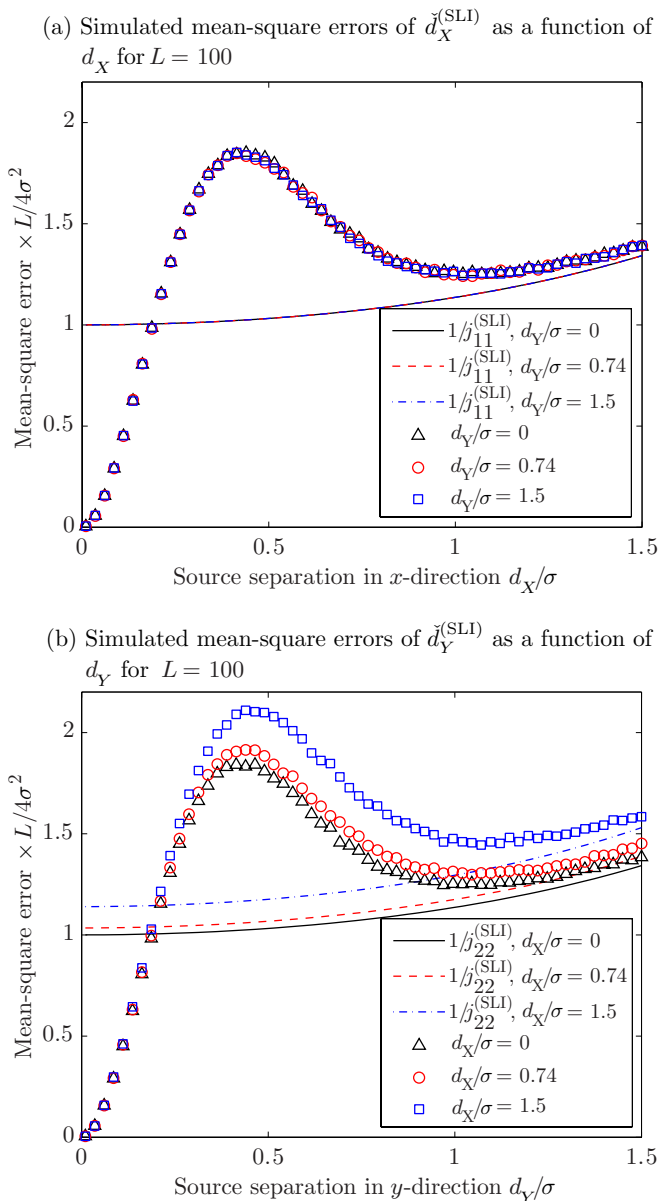


FIG. 6. Simulated mean-square errors of SLIVER with maximum likelihood estimators of Eq. (63) for different values of  $d_X$  and  $d_Y$  in  $L = 100$  trials. The corresponding Cramér-Rao bounds are included in the plots for comparison. (a) MSE of estimator  $\check{d}_X^{(\text{SLI})}$  as a function of the separation in  $x$ -direction for  $d_Y/\sigma = 0, 0.74, 1.5$ . (b) MSE of estimator  $\check{d}_Y^{(\text{SLI})}$  as a function of the separation in  $y$ -direction for  $d_X/\sigma = 0, 0.74, 1.5$ .

in Eq. (64) for  $\epsilon = 2 \times 10^{-3}$  photons. The ML estimators beat the Cramér-Rao bounds in the estimation of  $d_X$  and  $d_Y$  for small separations. The errors remain less than twice the Cramér-Rao bounds for any separations.

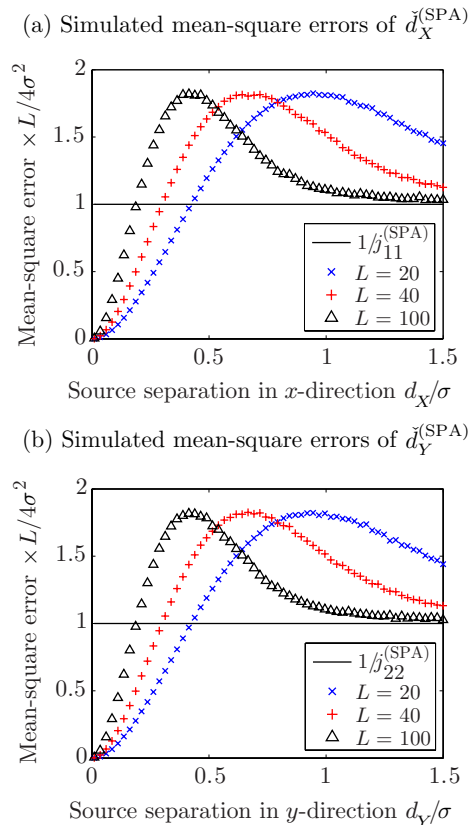


FIG. 7. Simulated mean-square errors of SPADE with maximum likelihood estimators of Eq. (64). (a) MSE of estimator  $\check{d}_X^{(\text{SPA})}$  as a function of the separation in  $x$ -direction for  $L = 20, 40, 100$  measurements. (b) MSE of estimator  $\check{d}_Y^{(\text{SPA})}$  as a function of the separation in  $y$ -direction for  $L = 20, 40, 100$  measurements.

## VII. DISCUSSION

In this paper, we have calculated the quantum Cramér-Rao bound for locating two weak incoherent optical point sources on a two-dimensional plane using imaging systems with inversion-symmetric point-spread functions. The key result is that, in stark contrast to direct imaging [8, 13], the bounds on the mean-square error of the  $x$ - and  $y$ -separations are independent of the vector separation between the two sources.

We have also proposed and analyzed two measurement schemes – the extended SLIVER and SPADE schemes – for simultaneously estimating the components of the separation, whose classical Cramér-Rao bounds approach the quantum bounds for sub-Rayleigh separations (SLIVER) or all separations if the PSF is Gaussian (SPADE). Monte-Carlo simulations show that the two schemes have MSEs no larger than twice predicted by the quantum limits for small source separation.

The extended SLIVER scheme given here does not employ an image inversion device (see, e.g., refs. [25, 26]), which was required in the scheme of ref. [15]. Thus, each

interferometer stage may be technically simpler to implement than the original SLIVER. However, the original scheme is tailored to estimation of the magnitude  $d = \sqrt{d_X^2 + d_Y^2}$  of the separation and is likely to be superior for that purpose than the two-stage scheme, as supported by the simulations in Sec. VI.

In both measurement schemes, we have assumed that the centroid position is known. If that knowledge is unavailable, a portion of the light can be used for image-plane photon counting to determine the centroid position before performing either of the schemes as detailed in ref. [13].

Our analysis here can be extended in various directions. On the theoretical side, our quantum Fisher information calculations can be extended to sources of arbitrary strength employing the Gaussian-state model [27, 28]. The study of sub-Rayleigh imaging can also be generalized to sources emitting light in more general quantum states [28]. In principle, it can also be extended to multiple sources, although finding near-optimal measurement schemes is likely to be challenging. On the practical side, it is important to study the performance of SLIVER and SPADE in non-ideal cases, e.g., if the centroid is not aligned to the optical axis in both schemes, or in the presence of non-unity coupling efficiency in SPADE, and for unequal detection efficiencies of the detectors.

## Appendix A: Quantum Fisher Information Matrix

To evaluate the QFI matrix, we first need to diagonalize  $\rho$  including enough eigenvectors to span the combined support of  $\rho$  and the  $\{\partial\rho/\partial\theta_\mu\}$ . The partial derivatives of  $\rho$  with respect to the object-plane source coordinates  $X_\mu$  and  $Y_\mu$  are

$$\frac{\partial\rho}{\partial X_\mu} = \frac{\partial D_1}{\partial X_\mu}|e_1\rangle\langle e_1| + \frac{\partial D_2}{\partial X_\mu}|e_2\rangle\langle e_2| + \left( D_1 \frac{\partial|e_1\rangle}{\partial X_\mu}\langle e_1| + D_2 \frac{\partial|e_2\rangle}{\partial X_\mu}\langle e_2| + \text{H.c.} \right), \quad (\text{A1})$$

$$\frac{\partial\rho}{\partial Y_\mu} = \frac{\partial D_1}{\partial Y_\mu}|e_1\rangle\langle e_1| + \frac{\partial D_2}{\partial Y_\mu}|e_2\rangle\langle e_2| + \left( D_1 \frac{\partial|e_1\rangle}{\partial Y_\mu}\langle e_1| + D_2 \frac{\partial|e_2\rangle}{\partial Y_\mu}\langle e_2| + \text{H.c.} \right), \quad (\text{A2})$$

where H.c. denotes the Hermitian conjugate. For  $\psi(x, y)$  symmetric about the origin, viz.,

$$\psi(x, y) = \psi(-x, -y), \quad (\text{A3})$$

we can show that the overlap  $\delta$  given by Eq. (5) is real-valued. After some algebra it can be shown that a possible set of eigenvectors of  $\rho$  is

$$\begin{aligned} |e_0\rangle &= |\text{vac}\rangle, & |e_1\rangle &= \frac{1}{\sqrt{2(1-\delta)}}(|\psi_1\rangle - |\psi_2\rangle), & |e_2\rangle &= \frac{1}{\sqrt{2(1+\delta)}}(|\psi_1\rangle + |\psi_2\rangle), \\ |e_3\rangle &= \frac{1}{c_3} \left[ \Delta k_X(|\psi_{1X}\rangle + |\psi_{2X}\rangle) + r_+ \Delta k_Y(|\psi_{1Y}\rangle + |\psi_{2Y}\rangle) - \frac{2(\gamma_X + r_+ \gamma_Y)}{\sqrt{2(1-\delta)}}|e_1\rangle \right], \\ |e_4\rangle &= \frac{1}{c_4} \left[ \Delta k_X(|\psi_{1X}\rangle + |\psi_{2X}\rangle) - r_+ \Delta k_Y(|\psi_{1Y}\rangle + |\psi_{2Y}\rangle) - \frac{2(\gamma_X - r_+ \gamma_Y)}{\sqrt{2(1-\delta)}}|e_1\rangle \right], \\ |e_5\rangle &= \frac{1}{c_5} \left[ \Delta k_X(|\psi_{1X}\rangle - |\psi_{2X}\rangle) + r_- \Delta k_Y(|\psi_{1Y}\rangle - |\psi_{2Y}\rangle) + \frac{2(\gamma_X + r_- \gamma_Y)}{\sqrt{2(1+\delta)}}|e_2\rangle \right], \\ |e_6\rangle &= \frac{1}{c_6} \left[ \Delta k_X(|\psi_{1X}\rangle - |\psi_{2X}\rangle) - r_- \Delta k_Y(|\psi_{1Y}\rangle - |\psi_{2Y}\rangle) + \frac{2(\gamma_X - r_- \gamma_Y)}{\sqrt{2(1+\delta)}}|e_2\rangle \right], \end{aligned} \quad (\text{A4})$$

where  $\delta$  is given by Eq. (5),  $\Delta k_X, \Delta k_Y, \gamma_X, \gamma_Y$  are defined in Eq. (19),

$$\begin{aligned} |\psi_{1X}\rangle &\equiv \frac{1}{\Delta k_X} \int_{-\infty}^{\infty} dx \int_{-\infty}^{\infty} dy \frac{\partial\psi(x - X_1, y - Y_1)}{\partial X_1} |x, y\rangle, \\ |\psi_{2X}\rangle &\equiv \frac{1}{\Delta k_X} \int_{-\infty}^{\infty} dx \int_{-\infty}^{\infty} dy \frac{\partial\psi(x - X_2, y - Y_2)}{\partial X_2} |x, y\rangle, \\ |\psi_{1Y}\rangle &\equiv \frac{1}{\Delta k_Y} \int_{-\infty}^{\infty} dx \int_{-\infty}^{\infty} dy \frac{\partial\psi(x - X_1, y - Y_1)}{\partial Y_1} |x, y\rangle, \end{aligned}$$

$$\begin{aligned} |\psi_{2Y}\rangle &\equiv \frac{1}{\Delta k_Y} \int_{-\infty}^{\infty} dx \int_{-\infty}^{\infty} dy \frac{\partial\psi(x - X_2, y - Y_2)}{\partial Y_2} |x, y\rangle, \\ c_3 &\equiv 2\sqrt{\Delta k_X^2 + b_X^2 - \frac{\gamma_X^2}{1-\delta} + |r_+| \left| a + a_s - \frac{\gamma_X \gamma_Y}{1-\delta} \right|}, \\ c_4 &\equiv 2\sqrt{\Delta k_X^2 + b_X^2 - \frac{\gamma_X^2}{1-\delta} - |r_+| \left| a + a_s - \frac{\gamma_X \gamma_Y}{1-\delta} \right|}, \end{aligned}$$

$$\begin{aligned}
c_5 &\equiv 2\sqrt{\Delta k_X^2 - b_X^2 - \frac{\gamma_X^2}{1+\delta} + |r_-| \left| a - a_s - \frac{\gamma_X \gamma_Y}{1+\delta} \right|}, \\
c_6 &\equiv 2\sqrt{\Delta k_X^2 - b_X^2 - \frac{\gamma_X^2}{1+\delta} - |r_-| \left| a - a_s - \frac{\gamma_X \gamma_Y}{1+\delta} \right|}, \\
r_{\pm} &\equiv \left[ \frac{\Delta k_X^2 \pm b_X^2 - \gamma_X^2 / (1 \mp \delta)}{\Delta k_Y^2 + b_Y^2 - \gamma_Y^2 / (1 \mp \delta)} \right]^{1/2} \\
&\quad \times \exp \left[ -i \arg \left( a \pm a_s - \frac{\gamma_X \gamma_Y}{1 \mp \delta} \right) \right], \\
a &\equiv \int_{-\infty}^{\infty} dx \int_{-\infty}^{\infty} dy \frac{\partial \psi^*(x, y)}{\partial x} \frac{\partial \psi(x, y)}{\partial y}, \\
a_s &\equiv \int_{-\infty}^{\infty} dx \int_{-\infty}^{\infty} dy \frac{\partial \psi^*(x, y)}{\partial x} \frac{\partial \psi(x - d_X, y - d_Y)}{\partial y}, \\
b_X^2 &\equiv \int_{-\infty}^{\infty} dx \int_{-\infty}^{\infty} dy \left[ \frac{\partial \psi^*(x - X_1, y - Y_1)}{\partial X_1} \right. \\
&\quad \left. \times \frac{\partial \psi(x - X_2, y - Y_2)}{\partial X_2} \right], \\
b_Y^2 &\equiv \int_{-\infty}^{\infty} dx \int_{-\infty}^{\infty} dy \left[ \frac{\partial \psi^*(x - X_1, y - Y_1)}{\partial Y_1} \right. \\
&\quad \left. \times \frac{\partial \psi(x - X_2, y - Y_2)}{\partial Y_2} \right], \tag{A5}
\end{aligned}$$

and the eigenvalues of  $\rho$  ( $D_n$  corresponding to  $|e_n\rangle$ ) are

$$\begin{aligned}
D_0 &= 1 - \epsilon, \quad D_1 = \frac{\epsilon}{2}(1 - \delta), \quad D_2 = \frac{\epsilon}{2}(1 + \delta), \\
D_3 &= D_4 = D_5 = D_6 = 0. \tag{A6}
\end{aligned}$$

The SLDs with respect to the derivative in Eqs. (A1) and (A2) can be found using Eq. (17),

$$\begin{aligned}
\mathcal{L}_{\mu}^{(X)} &= \sum_{\substack{m, n \\ D_m + D_n \neq 0}} \frac{2}{D_m + D_n} \langle e_m | \frac{\partial \rho}{\partial X_{\mu}} | e_n \rangle | e_m \rangle \langle e_n |, \\
\mathcal{L}_{\mu}^{(Y)} &= \sum_{\substack{m, n \\ D_m + D_n \neq 0}} \frac{2}{D_m + D_n} \langle e_m | \frac{\partial \rho}{\partial Y_{\mu}} | e_n \rangle | e_m \rangle \langle e_n |. \tag{A7}
\end{aligned}$$

Transforming to the centroid and separation parameters  $\theta$  of Eq. (7) gives the SLDs

$$\begin{aligned}
\mathcal{L}_1 &= \mathcal{L}_1^{(X)} + \mathcal{L}_2^{(X)}, \quad \mathcal{L}_2 = \mathcal{L}_1^{(Y)} + \mathcal{L}_2^{(Y)}, \\
\mathcal{L}_3 &= \frac{\mathcal{L}_2^{(X)} - \mathcal{L}_1^{(X)}}{2}, \quad \mathcal{L}_4 = \frac{\mathcal{L}_2^{(Y)} - \mathcal{L}_1^{(Y)}}{2}. \tag{A8}
\end{aligned}$$

We can now evaluate the quantum Fisher information using Eq. (16) to finally obtain Eq. (18).

## Appendix B: Fisher Information Matrix for SLIVER

Consider an arbitrary orthogonal basis  $\{|\varphi_q\rangle\}_{q=0}^{\infty}$  and define operator  $a_q$  as the annihilation operator that reduces the occupation number of the state  $|\varphi_q\rangle$  by 1. The

input field operator  $E(x, y)$  in Eqs. (25)–(28) can be expressed as

$$E(x, y) = \sum_{q=0}^{\infty} a_q \varphi_q(x, y), \tag{B1}$$

where

$$\varphi_q(x, y) = \langle x, y | \varphi_q \rangle, \tag{B2}$$

and state  $|x, y\rangle$  is as defined in Eq. (3). Using the following expression for  $a_q$ ,

$$a_q = \int_{-\infty}^{\infty} dx \int_{-\infty}^{\infty} dy E(x, y) \varphi_q^*(x, y), \tag{B3}$$

and the commutation relation  $[E(x, y), E^\dagger(x', y')] = \delta(x - x')\delta(y - y')$ , we have commutation relation

$$\begin{aligned}
[a_q, a_r^\dagger] &= \int_{-\infty}^{\infty} dx \int_{-\infty}^{\infty} dy \int_{-\infty}^{\infty} dx' \int_{-\infty}^{\infty} dy' \varphi^*(x, y) \\
&\quad \times \varphi(x', y') [E(x, y), E^\dagger(x', y')] \\
&= \int_{-\infty}^{\infty} dx \int_{-\infty}^{\infty} dy \varphi_q^*(x, y) \varphi_r(x, y) \\
&= \delta_{qr}. \tag{B4}
\end{aligned}$$

We can choose an orthogonal basis  $\{|\varphi_q\rangle\}$  with

$$|\varphi_0\rangle = |\psi_1\rangle, \tag{B5}$$

where state  $|\psi_1\rangle$  is given by Eq. (3). Hence, the field operator

$$E(x, y) = a_0 \psi_1(x, y) + \sum_{q=1}^{\infty} a_q \varphi_q(x, y), \tag{B6}$$

where wavefunction  $\psi_1(x, y)$  is given by Eq. (4). Similarly, we can have another orthogonal basis  $\{|\varphi'_q\rangle\}$  such that

$$|\varphi'_0\rangle = |\psi_2\rangle, \tag{B7}$$

and the field operator

$$E(x, y) = a'_0 \psi_2(x, y) + \sum_{q=1}^{\infty} a'_q \varphi'_q(x, y), \tag{B8}$$

where state  $|\psi_2\rangle$  is given by Eq. (3) and wavefunction  $\psi_2(x, y)$  is given by Eq. (4). The operators  $a_q$  and  $a'_r$  might not commute with one another, and the states  $|\varphi_q\rangle$  and  $|\varphi_r\rangle$  might not be orthogonal to each other. Using the expansion of  $E(x, y)$  in Eqs. (B6) and (B8) and the commutation relation in Eq. (B4), we can show that

$$\langle \psi_s | E(x, y) | \psi_s \rangle = 0, \quad s = 1, 2, \tag{B9}$$

$$\begin{aligned}
\langle \psi_s | E^\dagger(x, y) E(x', y') | \psi_s \rangle \\
= \psi_s^*(x, y) \psi_s(x', y') \quad s = 1, 2. \tag{B10}
\end{aligned}$$

The field operators at the open port of the two Mach-Zehnder interferometers,  $V_1(x, y)$  and  $V_2(x, y)$  of Eqs. (25)–(28), have the following expectation value in states  $|\psi_s\rangle$  for  $s = 1, 2$ :-

$$\langle \psi_s | V_q^\dagger(x, y) V_r(x', y') | \psi_s \rangle = 0, \quad q, r, s = 1, 2, \quad (\text{B11})$$

$$\langle \psi_s | V_r^\dagger(x, y) E(x', y') | \psi_s \rangle = 0, \quad r, s = 1, 2. \quad (\text{B12})$$

We can evaluate the probability of the  $r$ th detector clicks using Eq. (31) to obtain Eq. (32). Using Eq. (35) and the detection probability of Eq. (32) we can now evaluate the

Fisher information matrix and obtain Eq. (36).

## ACKNOWLEDGMENTS

S. Z. Ang, R. Nair and M. Tsang acknowledge support by the Singapore National Research Foundation under NRF Grant. No. NRF-NRFF2011-07 and the Singapore Ministry of Education Academic Research Fund Tier 1 Project R-263-000-C06-112.

- 
- [1] Lord Rayleigh, The London, Edinburgh, and Dublin Philosophical Magazine and Journal of Science **8**, 261 (1879).
- [2] E. Betzig, Opt. Lett. **20**, 237 (1995).
- [3] W. E. Moerner and L. Kador, Phys. Rev. Lett. **62**, 2535 (1989).
- [4] S. W. Hell and J. Wichmann, Opt. Lett. **19**, 780 (1994).
- [5] S. Weisenburger and V. Sandoghdar, Contemporary Physics **56**, 123 (2015).
- [6] E. Bettens, D. V. Dyck, A. den Dekker, J. Sijbers, and A. van den Bos, Ultramicroscopy **77**, 37 (1999).
- [7] S. V. Aert, A. den Dekker, D. V. Dyck, and A. van den Bos, Journal of Structural Biology **138**, 21 (2002).
- [8] S. Ram, E. S. Ward, and R. J. Ober, Proceedings of the National Academy of Sciences of the United States of America **103**, 4457 (2006).
- [9] H. L. Van Trees, *Detection, Estimation, and Modulation Theory Part. I* (John Wiley & Sons, New York, 2001).
- [10] C. W. Helstrom, *Quantum Detection and Estimation Theory* (Academic Press, New York, 1976).
- [11] A. S. Holevo, *Probabilistic and Statistical Aspects of Quantum Theory* (Edizioni della Normale, Pisa, Italy, 2011).
- [12] M. Tsang, Optica **2**, 646 (2015).
- [13] M. Tsang, R. Nair, and X.-M. Lu, (2015), arXiv:1511.00552 [quant-ph].
- [14] M. Tsang, R. Nair, and X.-M. Lu, arXiv:1602.04655 [quant-ph].
- [15] R. Nair and M. Tsang, Opt. Express **24**, 3684 (2016).
- [16] M. Hayashi, *Asymptotic Theory of Quantum Statistical Inference: Selected Papers* (World Scientific, 2005).
- [17] A. Fujiwara, Journal of Physics A: Mathematical and General **39**, 12489 (2006).
- [18] J. Goodman, *Introduction to Fourier Optics*, 3rd ed. (Roberts & Company Publishers, 2005).
- [19] H. Wiseman and G. Milburn, *Quantum Measurement and Control* (Cambridge University Press, 2010).
- [20] M. G. A. Paris, International Journal of Quantum Information **7**, 125 (2009).
- [21] L. Mandel and E. Wolf, *Optical Coherence and Quantum Optics* (Cambridge University Press, 1995).
- [22] J. Goodman, *Statistical Optics*, Wiley Series in Pure and Applied Optics (Wiley, 2000).
- [23] A. Yariv, *Quantum Electronics* (Wiley, New York, 1989).
- [24] K. Zhang and D. Li, *Electromagnetic Theory for Microwaves and Optoelectronics* (Springer Berlin Heidelberg, 2013).
- [25] K. Wicker, S. Sindbert, and R. Heintzmann, Optics Express **17**, 15491 (2009).
- [26] D. Weigel, H. Babovsky, A. Kiessling, and R. Kowarschik, Optics Communications **284**, 2273 (2011).
- [27] R. Nair and M. Tsang, (2016), arXiv:1604.00937 [quant-ph].
- [28] C. Lupo and S. Pirandola, ArXiv e-prints (2016), arXiv:1604.07367 [quant-ph].